Combustion Science and Technology
Publication details, including instructions for authors and subscription information:
http://www.tandfonline.com/loi/gcst20

Numerical Simulation of Ignition and Combustion of Ethylene in a Supersonic Model Combustor with a Reduced Kinetic Mechanism

Fengquan Zhong [a], Lihong Chen [a], Fei Li [a], Xinyu Zhang [a] & Chih-Jen Sung [b]

[a] State Key Laboratory of High Temperature Gas Dynamics, Institute of Mechanics, Chinese Academy of Sciences, Beijing, People's Republic of China

[b] University of Connecticut, Storrs, Connecticut, USA

Accepted author version posted online: 18 Oct 2012.Version of record first published: 29 Mar 2013.

To cite this article: Fengquan Zhong , Lihong Chen , Fei Li , Xinyu Zhang & Chih-Jen Sung (2013): Numerical Simulation of Ignition and Combustion of Ethylene in a Supersonic Model Combustor with a Reduced Kinetic Mechanism, Combustion Science and Technology, 185:4, 548-563

To link to this article: http://dx.doi.org/10.1080/00102202.2012.730080

Combust. Sci. Technol., 185: 548–563, 2013

ISSN: 0010-2202 print/1563-521X online
DOI: 10.1080/00102202.2012.730080

Taylor & Francis
Taylor & Francis Group

NUMERICAL SIMULATION OF IGNITION AND COMBUSTION OF ETHYLENE IN A SUPERSONIC MODEL COMBUSTOR WITH A REDUCED KINETIC MECHANISM

Fengquan Zhong,[1] Lihong Chen,[1] Fei Li,[1] Xinyu Zhang,[1] and Chih-Jen Sung[2]

[1]*State Key Laboratory of High Temperature Gas Dynamics, Institute of Mechanics, Chinese Academy of Sciences, Beijing, People's Republic of China*

[2]*University of Connecticut, Storrs, Connecticut, USA*

The unsteady process of ignition and combustion of ethylene at varied fuellair equivalence ratios in a Mach 2.5 supersonic model combustor is studied numerically. The reacting turbulent flow is solved using the shear stress transport (SST) k–ω turbulence model and a reduced kinetic mechanism obtained with sensitivity analysis and the assumption of quasi-steady-state from a detailed mechanism of ethylene. The present results reveal that ignition of ethylene first takes place in the cavity due to the local low speed and high static temperature. At a low equivalence ratio of 0.32, combustion is established and stabilized downstream of the cavity. However, as the equivalence ratio increases to 0.6, the combustion downstream of the cavity generates sufficient heat release to cause pressure and the flame to propagate upstream and to generate a shock train upstream of the injection point. Formation of the shock structure results in subsonic flow in the vicinity of the injection and combustion with higher efficiency stabilized mainly in the fuellair mixing shear layer. The time evolutions of fuel jet and C_2H_2 qualitatively agree well with the experimental results, of which high-speed schlieren photos and chemiluminescence images of CH^* are obtained at similar flow conditions.

Keywords: Ethylene; Ignition; Numerical simulation; Reduced kinetic mechanism; Supersonic combustion

INTRODUCTION

Hydrocarbons such as methane and ethylene are often used as fuel for scramjet applications such as the Hypersonic International Flight Research Experimentation (HIFiRE) project (Storch and Liu, 2011). Compared to hydrogen, ethylene has a longer ignition delay time and lower peak flame speed, which greatly affect the ignition reliability and combustion performance of ethylene. For supersonic

Received 18 July 2012; revised 10 September 2012; accepted 11 September 2012.

Address correspondence to Fengquan Zhong, State Key Laboratory of High Temperature Gas Dynamics, Institute of Mechanics, Chinese Academy of Sciences, Beijing 100190, People's Republic of China. E-mail: fzhong@imech.ac.cn

combustion at Mach numbers of 2–3, the characteristic ignition time of ethylene is approximately hundreds of microseconds to a few milliseconds, significantly larger than the characteristic time of small turbulent scales. Therefore, ignition and combustion of ethylene are essentially different from those of hydrogen and it is imperative that they are studied. At the same time, the relatively large reaction time of ethylene demands a qualified kinetic mechanism with good predictions of auto-ignition delay time and laminar flame speed for unsteady simulations.

For a numerical study of ethylene combustion, global reaction models with multiple steps and Arrhenius reaction rates are often used (Taha et al., 2002; Wang et al., 2008), but most global models are not able to describe the unsteady process of ignition accurately. So far, numerical simulations for supersonic combustion of ethylene using reduced mechanisms obtained from detailed mechanism via reduction methodology such as quasi-steady-state assumptions (QSS) are very limited and most of the available results are steady calculation (Gokulakrishnan et al., 2006; Montgomery et al., 2003), focusing on flow and reaction properties after the combustion is stabilized.

An effective unsteady simulation of supersonic combustion of hydrocarbons requires numerical schemes with high accuracy and a qualified turbulence model as well as a kinetic mechanism that can represent the interested chemical process. In addition, the computational demands of these combined models must be acceptable. Furthermore, considering the relatively large turbulence fluctuations in supersonic flow, especially in the vicinity of cavity or rearward facing step (used widely for ignition and flame holding in supersonic combustors as discussed by Ben-Yakar and Hanson, 2001), the interaction between turbulence and reactions is critical and must be modeled (Tishkoff et al., 1997).

In this article, ignition and combustion of ethylene in a supersonic model combustor with an inlet Mach number of 2.5 and total temperature of 1800 K is numerically studied via unsteady Favre-averaged Navier–Stokes (FANS) simulations with the shear stress transport (SST) k–ω model proposed by Menter (1994) with compressibility and low Reynolds number corrections. It is noted that while unsteady FANS cannot capture the small scale structures as compared to large eddy simulation (LES), it can still reasonably predict time changes of the large-scale phenomena of a chemically reacting flow such as flame propagation, formation of shock train structure, and dynamics of the fuel-air mixing, etc.

The chemistry is represented by a reduced kinetic mechanism based on the detailed mechanism of ethylene proposed by Wang and Laskin (1998). The chemistry-turbulence interaction is modeled using the eddy dissipation concept developed by Magnussen and Hjertager (1976). The present results show the time evolution of primary radicals and products as well as temperature field during the ignition, and also demonstrate that ignition at low and high equivalence ratios produce entirely different flow phenomena. The time evolution of C_2H_2 was found to be qualitatively consistent with experimental measurements, of which chemiluminescence images of CH^* at similar flow conditions were obtained.

This work is an attempt to study the unsteady process of ethylene ignition in supersonic conditions, and is expected to provide further insights into the ignition mechanism and combustion of hydrocarbons for scramjet applications.

NUMERICAL METHOD

The finite volume method is used to solve the Navier–Stokes equations and transport equations of species. The AUSM flux-splitting (Liou and Steffen, 1993) with third-order MUSCL scheme is applied for spatial discretization of the convective flux terms with low numerical dissipation and good performance of shock capturing. Viscous fluxes are approximated by a second-order central differencing scheme, and the time advancement is calculated by the implicit Euler method (cf. Weiss et al., 1997) with a time step of approximately 2×10^{-7} s. The SST k–ω model proposed by Menter (1994) with compressibility and low Reynolds number corrections is employed for the simulation of turbulence. The perfect gas assumption is used, and the NASA standard temperature polynomials have been used to determine the specific heat at constant pressure. Viscosity and thermal conductivity of species are calculated by kinetic theory with pre-given Lennard–Jones characteristic length and energy parameters. Fick's law governs mass diffusions, and the turbulent Schmidt number is set to 0.7. To validate the numerical scheme, the flow due to a nitrogen jet from a wall injector into a Mach 2.61 supersonic airflow was calculated. The normalized wall pressure is plotted in Figure 1a with comparison to experimental measurements of Spaid and Zukoski (1968), demonstrating good agreement. The bow shock and flow separation due to the injection and the Mach barrel structure of the jet are also clearly simulated, but they are not presented here for brevity. Since a cavity is often used in a supersonic combustor for ignition and flame holding, a cavity with a length-to-height ratio of 5 in a Mach 3 supersonic flow is also calculated. Figure 1b shows the distribution of the calculated wall pressure compared with the result reported by Gruber et al. (1999). The present numerical result agrees well with those of Gruber et al. (1999). The above two validations show that the present FANS simulations together with the turbulence model employed qualify for investigation of turbulent injection and mixing in a supersonic crossflow with a cavity.

The combustion/turbulence interaction is modeled by the method of eddy dissipation concept (EDC) developed by Magnussen and Hjertager (1976). The key idea of EDC is that chemical reactions with finite rates typically occur in vortices

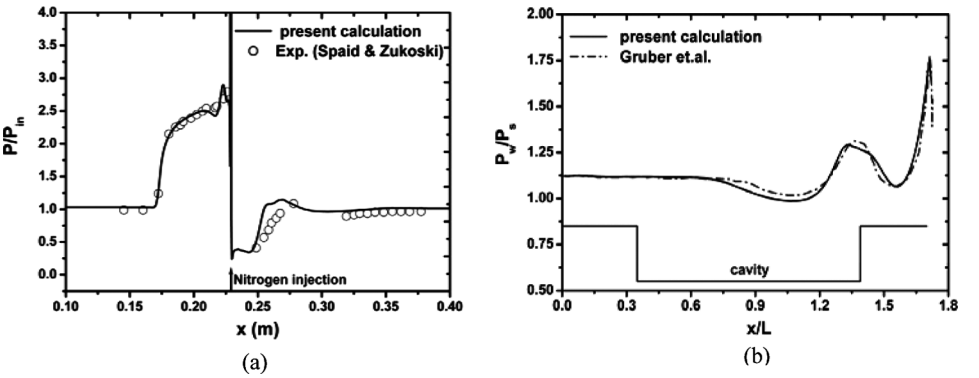

Figure 1 Validation of the numerical method: (a) distribution of normalized wall pressure of a jet flow; (b) distribution of normalized wall pressure of a cavity flow.

of turbulent flow, and the reaction rates are controlled by characteristic times of both the kinetic mechanism and the turbulence. With the EDC model, the kinetic mechanism can be fully coupled to the flow and temperature solver. However, the kinetic mechanism is inevitably somewhat stiff, and numerical integrations would become extremely computationally costly. To solve this problem, the in situ adaptive tabulation (ISAT) algorithm proposed by Pope (1997) is implemented to accelerate integrations and a speed up of approximately 40–50 times of the original computational speed can be achieved for the present cases.

COMPUTATIONAL DOMAIN AND BOUNDARY CONDITIONS

Figure 2 shows a two-dimensional model combustor with the following dimensions. The height of the combustor entrance is 50 mm, and the total length of the combustor is 860 mm. The combustor consists of a constant area section upstream of the cavity and a downstream divergent section with an angle of 2.4°. The length-to-height ratio of the cavity is 8 with an aft ramp angle of 27°. The computational domain is half of the combustor due to the symmetry of the combustor and flow in the vertical direction.

The flow condition at the entrance of the combustor is given as follows: Mach number 2.5, total temperature 1800 K, and static pressure 67 kPa; this represents a typical inlet condition of a scramjet combustor at flight Mach number of 6. Ethylene is injected on both the top and the bottom walls at a location 61 mm upstream of the cavity as indicated in the figure. The total temperature of ethylene is 1000 K, representing a thermally cracked state of hydrocarbon fuels such as kerosene (Lander and Nixon, 1971; Zhong et al., 2011). The total pressure of ethylene is varied according to pre-given fuel/air equivalence ratios.

The total mesh is 63,000 with 14,000 grid points in the cavity. The first grid point from the wall is at $\Delta y^+ \leq 1$, and there are eight points below $y^+ = 10$ for a fine mesh resolution near the wall. The mesh dependency was further investigated with either double or half the number of mesh points, showing no significant change in the simulated results.

REDUCED KINETIC MECHANISM OF ETHYLENE

The detailed mechanism for ethylene proposed by Wang and Laskin (1998) with 71 species and 395 reaction steps is first reduced to a skeletal mechanism including 30 species and 105 reaction steps by eliminating unimportant steps and redundant species. This skeletal reduction is accomplished by analyzing the perfectly

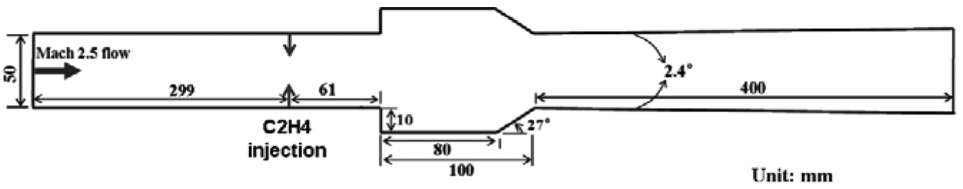

Figure 2 Schematic diagram of the Mach 2.5 supersonic combustor with injections of ethylene.

Table 1 A seven-step reduced kinetic mechanism of ethylene

Species	H_2, O_2, H, O, OH, CO, CO_2, H_2O, C_2H_2, C_2H_4, N_2
Reaction steps	$H + O_2 = O + OH$ $H_2 + O = H + OH$ $H_2 + OH = H + H_2O$ $2H = H_2$ $O + CO = CO_2$ $3H_2 + 2O + 2CO = 4H + 2O_2 + C_2H_2$ $2H_2 + H_2O + 2CO = H + O_2 + OH + C_2H_4$

stirred reactor (PSR) solutions (Glarborg et al., 1988) that contain information on species concentrations, rates of production, and species sensitivity coefficients to discern the relative importance of the elementary reaction steps (Chen, 1997; Sung et al., 1998). Using the QSS assumption (Chen, 1997; Peters, 1991), QSS species in the skeletal mechanism are indentified and their rates of formation can be determined algebraically by the non-QSS species concentrations, temperature, and pressure. The present reduced mechanism consists of 11 species and 7 steps, as listed in Table 1. It is worthy mentioning that such a reduced mechanism is different from commonly used multiple-step models with pre-given Arrehenius parameters. The global reaction rates in a reduced mechanism are expressed in terms of the elementary reaction rates that usually are functions of the QSS species.

Figure 3a plots the auto-ignition delay time (atmospheric conditions, fuel/air equivalence ratio of 1.0) as a function of temperature determined by the reduced mechanism, the skeletal mechanism, as well as the experimental data of Horning (2001). The ignition delay time predicted by the reduced mechanism is found to be smaller than the experimental data with discrepancies less than 36%. Figure 3b gives the variation of laminar flame speed as a function of fuel/air equivalence ratio at a mixture temperature of 298 K and a pressure of 1 atm. A satisfactory agreement is observed between the predictions and the experimental data obtained by Egolfopoulos et al. (1991), with the maximum discrepancy being 12%.

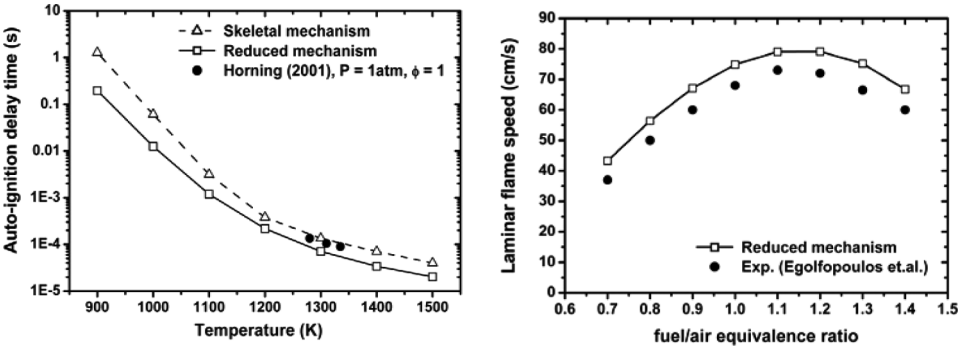

Figure 3 Comparison of predictions by the reduced mechanism to the experimental data. (a) auto-ignition delay time and (b) laminar flame speed.

RESULTS AND DISCUSSIONS

Ignition of Ethylene at Overall Fuel/Air Equivalence Ratio of 0.32

The ethylene is injected at sonic speed, a total pressure of 3.5 atm, and a total temperature of 1000 K. Considering ethylene is one of the major products of thermally cracked hydrocarbon fuels such as kerosene (Lander and Nixon, 1971), the high preheat temperature of ethylene represents the cracking temperature. The overall fuel/air equivalence ratio in this case is 0.32.

The computed physical time for ethylene ignition and combustion is 13 ms, and a steady state was reached at approximately $t = 6$ ms. Figure 4 presents a time development of the static temperature of the flow. As shown in the figure, ignition of ethylene (denoted by a local high temperature region) first occurs in the cavity during $t = 0.8$–1.35 ms, and at $t = 1.35$ ms, ethylene is found to be ignited downstream of the cavity. From $t = 2$ ms, combustion of ethylene is being established downstream of the cavity and, at $t = 6$ ms, the ignition nearly reaches completion, which is verified by comparing distributions of pressure or fractions of species at different moments. The ignition process can be also described by the time evolution of the formation rate (in kg/m^{3}s) of OH, ω_{OH}, as shown in Figure 5. At $t = 1.35$ ms, a significant formation of OH is found downstream of the cavity, denoting the main ignition region. The OH formation is gradually stabilized downstream of the cavity after $t = 2$ ms. Figure 6 shows the time development of formation rate (in kg/m^{3}s) of C_2H_2, a key intermediate during the ignition process. From $t = 2$ ms, consumption of C_2H_2, expressed by the negative value of $\omega_{C_2H_2}$, is found just downstream of the cavity.

The mass fraction contours of H_2O, CO, and CO_2 after the completion of ignition ($t = 13$ ms) are presented in Figure 7. H_2O and CO are produced mostly in the cavity and just downstream of the cavity. CO_2, however, is generated far downstream due to its longer residence time and more sufficient mixing between fuel and oxygen required for its formation.

Figure 8 gives the contours of Mach number and static pressure, respectively. As shown by the contours of Mach number, the bow shock caused by the fuel

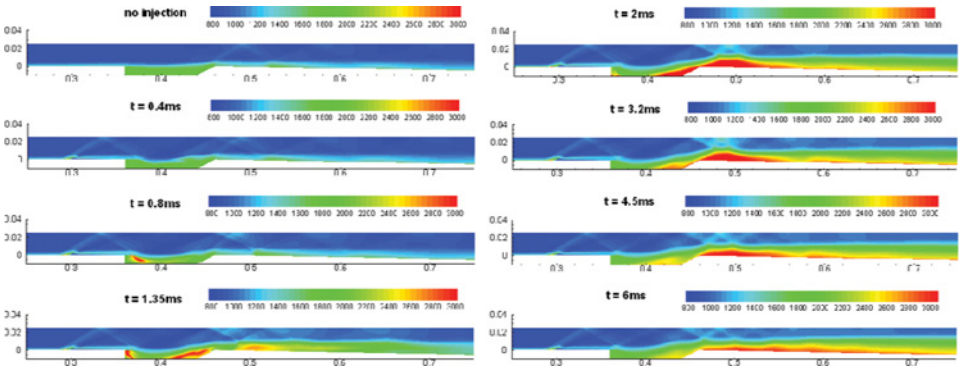

Figure 4 Sequence of the contours of static temperature in Kelvin. (*Note*: the beginning of the x-coordinate is not from zero.) (Figure is provided in color online.)

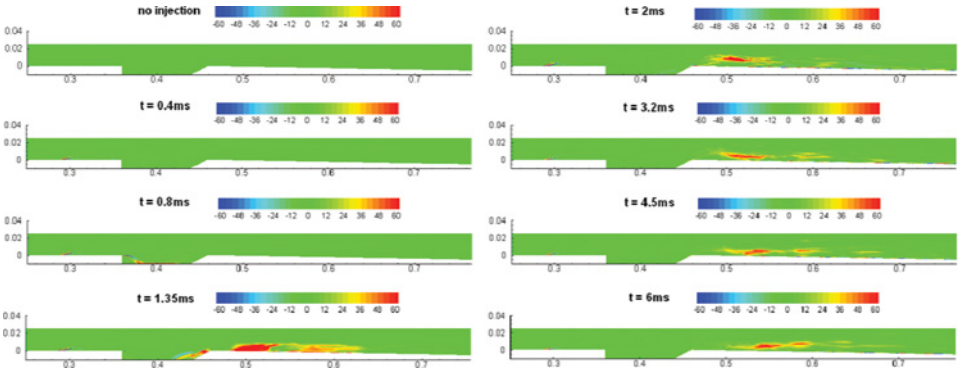

Figure 5 Sequence of the contours of formation rate of OH in units of kg/m^{3}s. (Figure is provided in color online.)

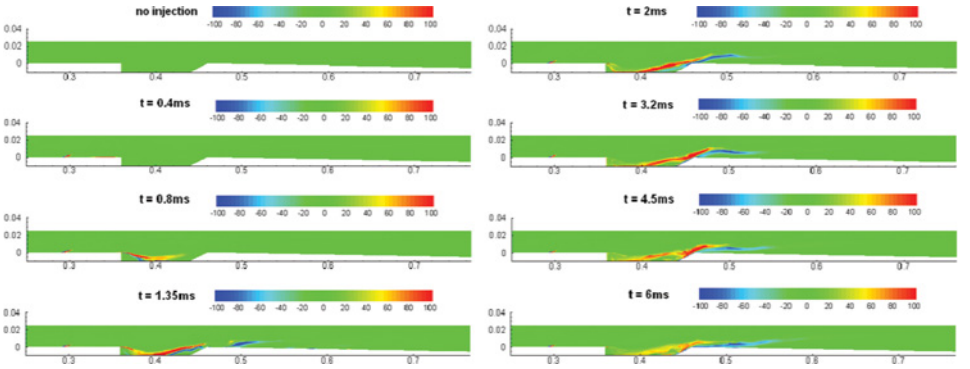

Figure 6 Sequence of the contours of formation rate of C_2H_2 in units of kg/m^{3}s. (Figure is provided in color online.)

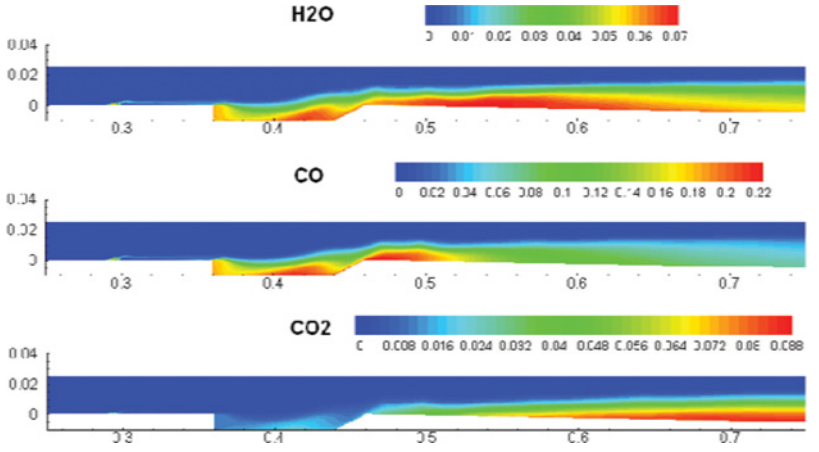

Figure 7 Contours of mass fraction of H_2O, CO, and CO_2 at t = 13 ms. (Figure is provided in color online.)

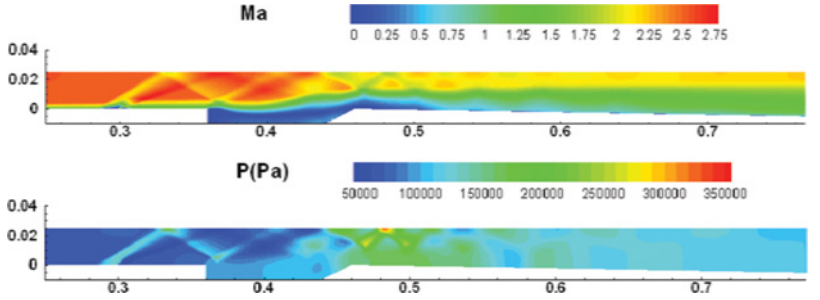

Figure 8 Contours of Mach number and pressure at t = 13 ms. (*Note*: the beginning of the x coordinate is not from zero.) (Figure is provided in color online.)

injection is well captured. The reflection of shock waves from the above boundary indicates that the combustion is mainly supersonic. Contours of pressure show that the maximum pressure is located downstream of the cavity, corresponding to the major combustion region.

Ignition of Ethylene at Overall Fuel/Air Equivalence Ratio of 0.6

Ignition of ethylene at an overall fuel/air equivalence ratio of 0.6 is simulated with a total physical time of 17 ms. Figure 9 shows the time evolution of static temperature. The ignition at this higher fuel/air ratio is found to be much more complicated than that at a lower fuel/air ratio. Similar to the results for an equivalence ratio of 0.32, at t = 0.8 ms, ethylene initially ignites in the cavity, and, from t = 1.4 ms, the major ignition occurs just downstream of the cavity. However, with a higher fuel/air equivalence ratio, combustion of ethylene is not stable downstream

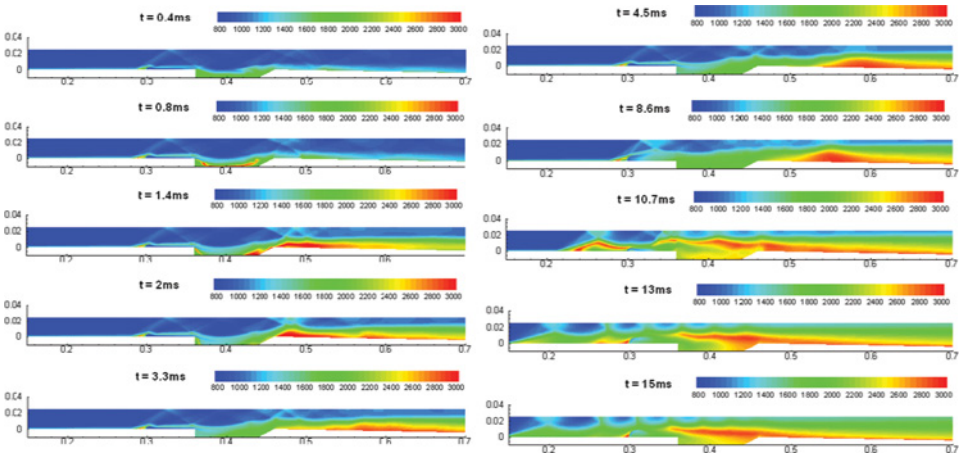

Figure 9 Time evolution of the contours of static temperature in Kelvin at equivalence ratio of = 0.6. (*Note*: the beginning of the x coordinate is not from zero.) (Figure is provided in color online.)

of the cavity; instead, the combustion flame propagates upstream during the period of t = 4.5–10.7 ms. Propagation of the flame is caused by imbalance of pressures at the combustor inlet and downstream of the cavity since significant heat release of the combustion raises the downstream pressure. The flame movement even disturbs the fuel jet and forces it to be oriented towards the upstream direction within a very short time. This reversing of the fuel jet causes some of the fuel to diffuse upstream of the injection and react rapidly because of the locally high static temperature. As the fuel jet returns back to its normal position and the small amount of fuel upstream of the injection has been burned out, the ignition process gradually becomes stable with a shock train generated upstream of the injection (in the so-called ''isolator'' of the combustor as described by Heiser and Pratt, 1994).

Figure 10 gives the contours of density and shows the time development of the fuel jet during a short period of 0.9 ms. Within this period, the fuel jet is forced to be oriented upstream by the propagation of the combustion and shock waves before recovering. The same phenomenon is observed in experiments at similar flow conditions as discussed in our previous report (Chen et al., 2012; Li et al., 2011). Figure 11 shows a sequence of high-speed schlieren images in a time interval of 0.6 ms, and it clearly shows the same jet movements as the combustion and shock waves move upstream.

The time development of the formation rate of OH is shown in Figure 12. Compared to that of the lower fuel/air ratio case, during the early period of $t \leq 4.5$ ms, the evolution of ω_{OH} is similar, showing that ignition initially occurs in the cavity, then the major ignition takes place downstream of the cavity. The difference, however, appears at t = 6 ms when the peak of ω_{OH} propagates upstream and, at approximately t = 15 ms, it is stabilized and located above and across the cavity and in the fuel/air mixing shear layer. In Figure 12, the picture at t = 15 ms shows that the formation of OH is mainly located downstream of the injection and in the mixing shear layer, indicating a ''jet-wake stabilized'' combustion as identified

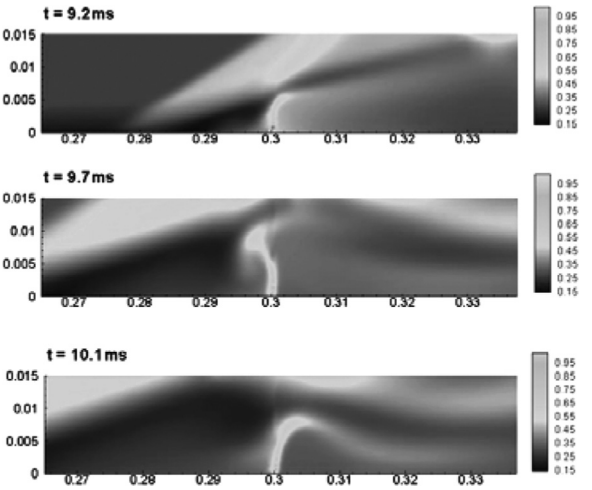

Figure 10 Time evolution of the density of the flow (in units of kg/m^3) during a period of 0.9 ms.

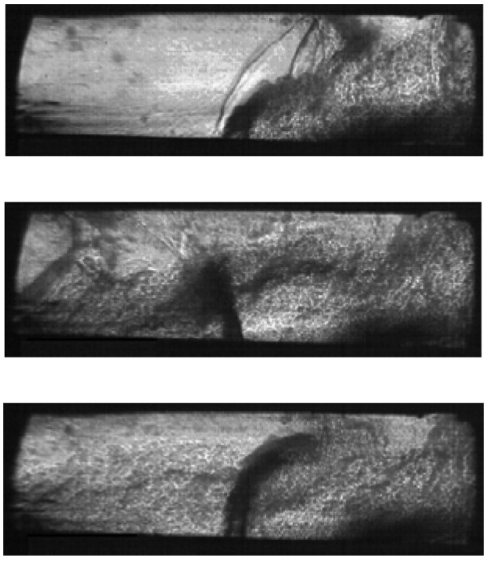

Figure 11 Sequence of the motion of fuel jet with high-speed schlieren images.

by Micka et al. (2009). A comparison of Figures 5 and 12 reveals that distance from the injection to the primary formation of OH at equivalence ratio of 0.6 is much shorter than that at equivalence ratio of 0.32, which can be attributed to the change in the flow field near the injection due to the shock train and boundary layer separation.

Figures 13a–13c present the contours of mass fraction of C_2H_2 at various times. As shown in Figure 13a at $t = 3.6$ ms, C_2H_2 is mainly located in the downstream part of the cavity, similar to the result obtained at the lower fuel/air ratio. As time increases to 10 ms, a small portion of C_2H_2 exists upstream of the injection due to the turning of the fuel jet in the period of $t = 9.2$–10.1 ms as shown in Figure 10. At this moment, C_2H_2 is found mainly in the cavity. As time advances to 12 ms, the majority of C_2H_2 is distributed at the leading edge and in the front part of the cavity as shown in Figure 13c. Images of CH^* chemiluminescence

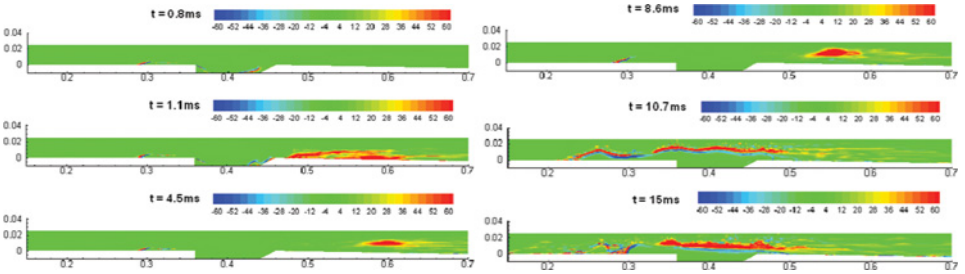

Figure 12 Time development of the formation rate of OH in units of kg/m^{3}s. (*Note*: the beginning of the x coordinate is not from zero.) (Figure is provided in color online.)

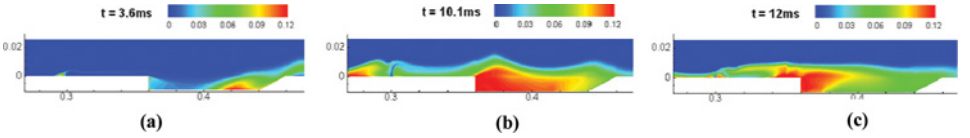

Figure 13 Contours of mass fraction of C_2H_2 at various times. (Figure is provided in color online.)

(indicating concentration of CH) during ignition at similar flow and fuel conditions are given in Figures 14a–14c, which show a similar time evolution. It is noted that the time concentration variations of CH and C_2H_2 are found to be close to each other from the analysis of the perfectly stirred reactor. The chemiluminescence from CH^* is imaged using a 9.9 nm half-bandwidth filter centered at 430 nm and recorded with a CCD camera with an exposure time of 1 ms. More details of this optical setup for the chemiluminescence images are described by Chen et al. (2012). The three chemiluminescence images of CH^* show the change of CH as the flame propagates upstream. The qualitative agreement between the numerical and the experimental results validates the present simulation of the unsteady ignition process.

Figure 15a shows the contours of Mach number at t = 17 ms, when the flow and combustion reach a steady state. The shock train structure is clearly identified upstream of the injection, and it causes locally significant boundary layer separation and deceleration of the flow near the injection. Figure 15b gives the sonic line; the subsonic flow in the vicinity of injection is clearly shown. The much lower flow speed and longer residence time for the fuel explain the short distance from the injection to the peak of ω_{OH} as shown in Figure 12.

Figures 16a–16c show the contours of the mass fraction of H_2O, CO, and CO_2, respectively, at t = 17 ms. Compared to those for the lower fuel/air ratio case (cf. Figure 7), H_2O, CO, and CO_2 are located further upstream due to low flow speed and high static temperature near the injection and therefore an earlier and faster combustion.

At the combustor exit, an overall combustion efficiency proposed by Heiser and Pratt (1994) is defined as follows:

$$\eta_b = \frac{H_e - H_i}{\dot{m}_{air} f h_{PR}} \tag{1}$$

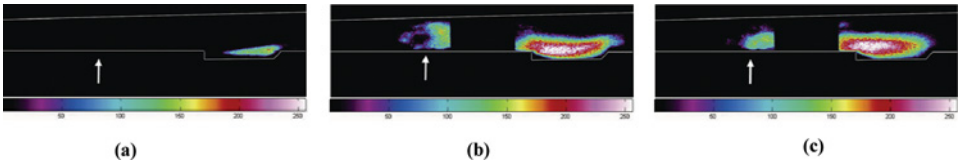

Figure 14 Experimental images of CH^* chemiluminescence during the ethylene ignition. (The black region between the CH chemiluminescences is a metal side wall of the combustor.) (Figure is provided in color online.)

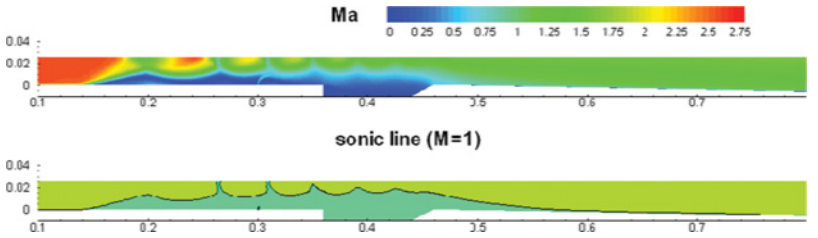

Figure 15 Contours of flow Mach number for the higher fuel/air ratio case. (*Note*: the beginning of the x coordinate is not from zero.) (Figure is provided in color online.)

where f is the stoichiometric fuel/air mass ratio, h_{PR} is heating value of the fuel, $\dot{m}_{air}$ is the inlet mass flow rate, and H_e and H_i denote the mass-averaged enthalpy of the flow at the exit and at the inlet of the combustor, respectively; they are defined by $H = \int \rho uh\, dy$.

The present results give the combustion efficiency at the model combustor exit of 0.6 for the lower fuel/air ratio case and 0.82 for the higher fuel/air ratio case. The relatively large combustion efficiency of 0.82 for the latter case is not surprising, since the shock train structure formed upstream of the injection causes the flow to slow to nearly subsonic, and combustion is more complete with a longer residence time and higher static temperature.

Using mass averaging as defined by $A = \int \rho ua\, dy$, distributions of flow properties along the combustor are given as follows for a more straightforward understanding of the combustion. Figures 17a and 17b show the mass-averaged Mach number and total temperature for the two cases. At the overall equivalence ratio of 0.6, oscillation of Mach number from x = 0.15 m to the cavity is found, which is caused by the shock train and the boundary layer separation. Downstream of the injection, the lowest Mach number for the higher fuel/air ratio case is smaller than 1, indicating that combustion occurs mainly in the subsonic flow regime. The total temperature

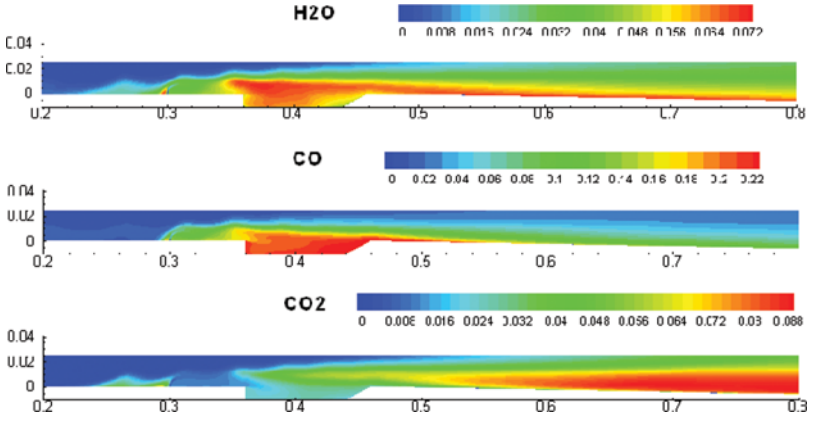

Figure 16 Contours of mass fractions of H_2O, CO, and CO_2 for the higher fuel/air ratio case. (Figure is provided in color online.)

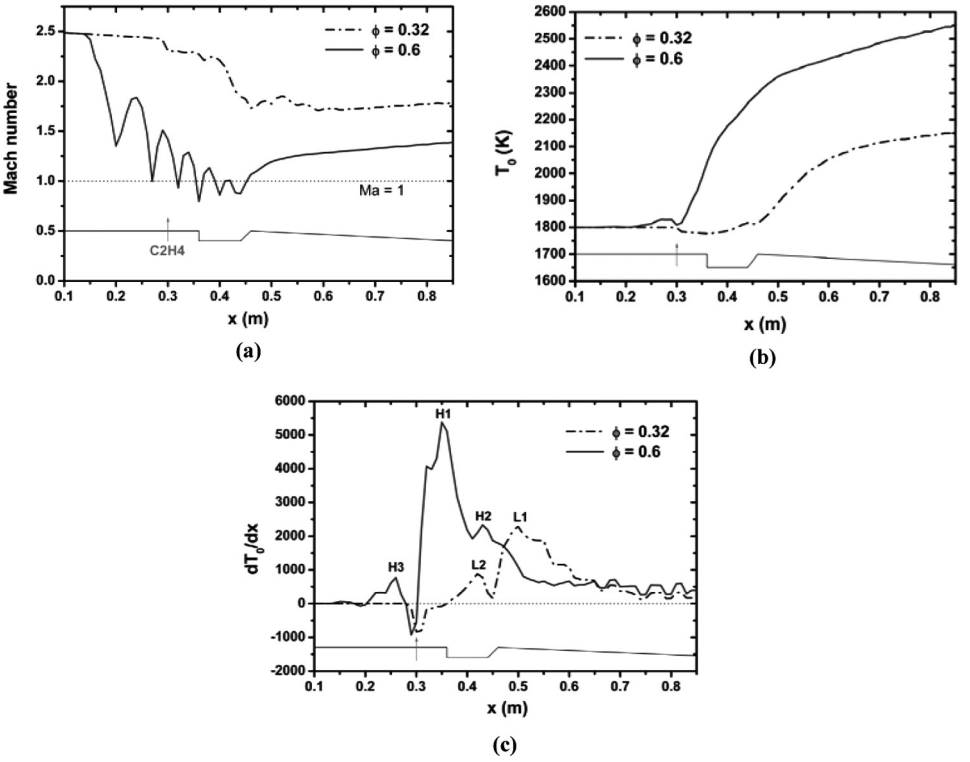

Figure 17 Distribution of mass-averaged flow properties along the combustor: (a) Mach number, (b) total temperature, (c) dT_0/dx in K/m.

curves of Figure 17b show that the increase in total temperature of the higher fuel/air ratio case occurs significantly earlier than that of the lower fuel/air ratio case, revealing a faster combustion heat release. The rate of heat release can be identified more clearly by plotting $\frac{dT_0}{dx}$ along the combustor length as given in Figure 17c. At the equivalence ratio of 0.32, the maximum $\frac{dT_0}{dx}$ (denoted by L1 in the figure) is located downstream of the cavity, corresponding to the formation rate of OH as indicated in Figure 5 at $t = 6$ ms; the combustion is cavity stabilized. A second peak of $\frac{dT_0}{dx}$ (denoted by L2) with a smaller value occurs in the rear part of the cavity, indicating locally weak combustion. At the equivalence ratio of 0.6, three peaks can be identified (denoted as H1, H2, and H3 in the figure), among which the maximum of $\frac{dT_0}{dx}$, H1, is located just downstream of the injection and in the fuel/air mixing shear layer, representing a typical "jet-wake stabilized" combustion. In this case, the cavity still works as a flame holder, implicated by the existence of the second peak, H2, with smaller value of $\frac{dT_0}{dx}$ than H1. The third peak, H3, appears upstream of the injection as a result of a small portion of fuel being rolled upstream and burned rapidly due to the high static temperature in front of the jet stagnation point. The present results of ethylene ignition and combustion at varied fuel/air equivalence ratios reveal differences in the mechanism of supersonic burning and in the distribution of heat release.

SUMMARY

In this article, the unsteady processes of ignition and combustion of heated ethylene in a Mach 2.5 supersonic model combustor are numerically studied. The flow is solved using a numerical scheme with adequate shock capturing, as well as the turbulence model with low Reynolds number and compressibility corrections. Using the quasi-steady-state assumption (QSS), the detailed kinetic mechanism proposed by Wang and Laskin (1998) is reduced to an acceptable size for a multidimensional computation. The eddy dissipation concept (EDC) of fully coupling the flow solver and chemical reaction is applied to model turbulence/chemistry interaction, and the in situ adaptive tabulation (ISAT) approach is used to speed up the computation.

Based on the current numerical results, a few conclusions can be drawn as follows:

1. Supersonic ignition of ethylene at varied fuel/air equivalence ratios is essentially different. For the present flow and fuel conditions, the physical time for the completion of ignition at equivalence ratio of 0.32 is approximately 6 ms, much shorter than the 15 ms at equivalence ratio of 0.6 (cf. Figures 4, 5, 6, 9, and 12).
2. For both cases, the initial ignition occurs in the cavity (cf. Figures 4 and 9). For the lower fuel/air equivalence ratio case, the major ignition and stabilized combustion are located downstream of the cavity (cf. Figures 4 and 5). The higher equivalence ratio case, however, presents a more complicated process where the combustion downstream of the cavity and the associated pressure rise cause the combustion wave to propagate upstream (cf. Figures 9 and 12) and the shock train structure is formed (cf. Figures 10 and 11). During the flame propagation, the fuel jet is forced to be oriented upstream for a short period (less than 1 ms), which is observed by both the numerical and the experimental results (cf. Figures 10 and 11).
3. At higher fuel/air equivalence ratio, formation of the shock train and boundary layer separation cause the fuel mixing and combustion to occur in subsonic flow conditions, thereby significantly increasing the combustion efficiency (cf. Figures 9, 15, and 16).
4. The mass-averaged flow properties reveal that distributions of heat release are different for the lower and the higher fuel/air ratio cases (cf. Figures 5, 12, and 17). The heat release at equivalence ratio of 0.32 is mainly located downstream of the cavity, representing a cavity-stabilized combustion. At equivalence ratio of 0.6, the heat release has two major peaks: one in the fuel/air mixing layer and another in the rear part of the cavity. The equivalence ratio of the 0.6 case indicates that combustion is mainly jet-wake stabilized and the flame-holding effect of the cavity is diminished.

In the present study, a two-dimensional combustor is used as a model, and hence the three-dimensional effects (especially jet lateral spreading) are not considered. Therefore, a three-dimensional numerical follow-up study is currently underway.

ACKNOWLEDGMENTS

This work is funded by Natural Science Foundation of China under Contract No. 10921062 and 11172309. The authors would like to thank Professor Gong Yu of

Chinese Academy of Sciences for his help in this work. C.J.S. is also supported by the China's Programme of Introducing Talents of Discipline to Universities–111 Project under Grant No. B08009 and the Thousand Talents Program.

REFERENCES

Ben-Yakar, A., and Hanson, R.K. 2001. Cavity flame-holders for ignition and flame stabilization in scramjets: An overview. *J. Propul. Power*, **17**(4), 869–877.

Chen, J.-Y. 1997. Development of reduced mechanisms for numerical modeling of turbulent combustion. Presented at the Workshop on Numerical Aspects of Reduction in Chemical Kinetics, CERNICS-ENPC, Cite Descartes, Champus sur Marne, France.

Chen, L.-H., Li, F., Wan, T., Li, Z., and Gu, H.-B. 2012. Interaction between combustion and shock wave in supersonic combustor. In *28th International Symposium on Shock Waves*, K. Kontis (Ed.), Vol. 2, Springer-Verlag, Berlin, pp. 313–318.

Egolfopoulos, F.N., Zhu, D.L., and Law, C.K. 1991. Experimental and numerical determination of laminar flame speeds: Mixtures of C_2-hydrocarbons with oxygen and nitrogen. *Symp. (Int.) Combust.*, **23**, 471–478.

Glarborg, P., Kee, R.J., Grcar, J.F., and Miller, J.A. 1988. PSR: A FORTRAN program for modeling well stirred reactors. Sandia National Laboratories Report 86-8209.

Gokulakrishnan, P., Pal, S., Klassen, M.S., Hamer, A.J., Roby, R.J., Kozaka, O., and Menon, S. 2006. Supersonic combustion simulation of cavity-stabilized hydrocarbon flames using ethylene reduced kinetic mechanism. AIAA Paper 2006-5092.

Gruber, M.R., Baurle, R.A., Mathur, T., and Hsu, K-Y. 1999. Fundamental studies of cavity-based flameholder concepts for supersonic combustors. AIAA Paper 1999-2248.

Heiser, W.H., and Pratt, D.T. 1994. *Hypersonic Airbreathing Propulsion*, American Institute of Aeronautics and Astronautics, Inc., Washington, DC, Chap. 3 and Chap. 6.

Horning, D.M. 2001. A study of the high-temperature auto-ignition and thermal decomposition of hydrocarbons. Report No. TSD-135, Stanford University.

Lander, H., and Nixon, A.C. 1971. Endothermic fuels for hypersonic vehicles. *J. Aircr.*, **8**(4), 200–207.

Li, F., Li, Z., Gu, H.-B., Yu, X.-L., Chen, L.-H., and Chang, X.-Y. 2011. Combustion oscillation in a dual-mode scramjet combustor at low Mach number. Presented at the The 4th Hypersonic Technology Conference of China, CSTAM 2011-2745, December 6–8, Sanya.

Liou, M.S., and Steffen, Jr., C.J. 1993. A new flux splitting scheme. *J. Comput. Phys.*, **107**, 23–39.

Magnussen, B.F., and Hjertager, B.H. 1976. On mathematical models of turbulent combustion with special emphasis on soot formation and combustion. *Proc. Combust. Inst.*, **16**(1), 719–729.

Menter, F.R. 1994. Two-equation eddy-viscosity turbulence models for engineering applications. *AIAA J.*, **32**(8), 1598–1605.

Micka, D.J., Torrez, S.M., and Driscoll, J.F. 2009. Heat release distribution in a dual-mode scramjet combustor—measurements and modeling. AIAA Paper 2009–7362.

Montgomery, C.J., Zhao, W., Tam, C.-J., Eklund, D.R., and Chen, J.-Y. 2003. CFD simulation of a 3-D scramjet flameholder using reduced chemical kinetic mechanisms. AIAA Paper 2003–3874.

Peters, N. 1991. *Reducing Mechanisms*, Springer-Verlag, Berlin.

Pope, S.B. 1997. Computationally efficient implementation of combustion chemistry using in-situ adaptive tabulation. *Combust. Theor. Model.*, **1**, 41–63.

Spaid, F.W., and Zukoski, E.E. 1968. A study of the interaction of gaseous jets from transverse slots with supersonic external flows. *AIAA J.*, **6**(2), 205–212.

Storch, A., and Liu, J. 2011. Combustor operability and performance verification for HIFiRE Flight 2. AIAA Paper 2011-2249.

Sung, C.J., Law, C.K., and Chen, J.-Y. 1998. An augmented reduced mechanism for methane oxidation with comprehensive global parametric validation. *Proc. Combust. Inst.*, **27**, 295–304.

Taha, A.A., Tiwari, S.N., and Mohieldin, T.O. 2002. Combustion characteristics of ethylene in scramjet engines. *J. Propul. Power*, **18**(3), 716–718.

Tishkoff, J.M., Drummond, J.P., and Edwards, T. 1997. Future directions of supersonic combustion research. Air Force/NASA Workshop on Supersonic Combustion, AIAA Paper 1997-1017.

Wang, D., Song, W.Y., Cao, Y.J., and Cai, Y.H. 2008. Numerical research on the influence of different step and expanding modes on scramjet combustor. *Comput. Simul.*, **25**(10), 82–85.

Wang, H., and Laskin, A. 1998. A comprehensive kinetic model of ethylene and acetylene oxidation at high temperatures. Progress Report for an AFOSR New World Vista Program, University of Delaware, Newark, DE.

Weiss, J.M., Maruszewski, J.P., and Smith, W.A. 1997. Implicit solution of the Navier-Stokes equations on unstructured meshes. AIAA paper 1997-2103.

Zhong, F.-Q., Fan, X.-J., Yu, G.., Li, J.-G., and Sung, C.J. 2011. Thermal cracking and heat sink capacity of aviation kerosene under supercritical conditions. *J. Thermophys. Heat Transfer*, **25**(3), 450–456.